On the reassessment of bridge superstructure vibrations for high-speed traffic

Patrick Simon[1[0000-0002-1538-177X]] and Matthias Baeßler[1[0000-0002-5182-7310]]

[1] Bundesanstalt für Materialforschung und -prüfung (BAM), Berlin, Germany
patrick.simon@bam.de

Abstract. The acceleration thresholds of bridge superstructures remain critical for designing and reassessing railway bridges on high-speed lines, with ballasted track systems historically limited to 3.5 m/s² vertical accelerations due to destabilization risks. As part of the European InBridge4EU project, this study addresses methodological uncertainties in linking vertical bridge vibrations to lateral track creep—a key focus area for modernizing assessment protocols. A comparative analysis of two acceleration postprocessing methods (peak identification vs. fatigue-derived rainflow counting) as part of a recently proposed framework was conducted using an example bridge and train combination. Results demonstrate that rainflow counting yields more conservative creep estimates with the bulk of cumulative vibration-induced creep attributable to accelerations exceeding 3 m/s². However, discretizing acceleration ranges into 1 m/s² bins introduced significant errors compared to continuous cycle data, highlighting sensitivity to analysis parameters. These findings underscore the complexity of reconciling laboratory-derived harmonic vibration models with real-world bridge dynamics, where non-uniform acceleration patterns dominate. The research directly informs ongoing efforts to refine standardized criteria for ballasted track stability, particularly through the InBridge4EU project's systematic re-evaluation of vibration limits and their engineering implications. By quantifying discrepancies between computational approaches, this work advances the development of robust protocols for predicting track degradation under high-speed operational loads.

Keywords: Infrastructure, Railway Bridges, Ballasted Track, Railway Bridge Dynamics, Rainflow Counting.

1 Introduction

Railway bridges are crucial for supporting railway tracks, and their design is heavily influenced by the interaction between the vehicle, track, and bridge. Service limit states, which ensure traffic safety, often dictate the design [1]. Limiting deflections of bridge superstructures are necessary for passenger comfort, but certain vehicle-track combinations can cause structural resonances, causing significant vibrations.

Historical observations from the commissioning the Paris–Lyon line [2], showed that large vibration amplitudes of greater than 0.7 g occurred which lead to a destabilization of the ballasted track, causing lateral track shifts. This phenomenon of ballast destabilization lead to the definition of a limit criterion of 0.35 g for the vertical acceleration amplitudes of bridges with ballasted track, such as found in [3].

Destabilization of ballasted track due to dynamic actions is critical, especially when vertical vibrations of the bridge act on the track while at the same time, lateral static loads of the track act on the sleepers, causing vibration-induced creep [4, 5].

Existing literature examines either the bridge-train dynamics [6, 7, 8] or the lateral track resistance [9], but the combined actions of vertical vibrations of the bridge and lateral forces on the sleepers remains unexplored.

A recently proposed assessment for the stability of ballasted track on vibrating bridge decks [10] aims to bridge this gap by quantifying the effects of bridge vibrations on track stability. This approach utilizes a dynamic train-bridge model for the vertical vibrations and a horizontal track model for the lateral forces acting on the sleepers. Both results are related via a formula for the vibration-induced creep derived from laboratory experiments [4, 5]. A recent master's thesis [11] applied rainflow counting to this problem as an analogy from fatigue analysis. However, there is significant uncertainty in the postprocessing of the vertical accelerations of the dynamic train-bridge model and the way these are related to the laboratory tests, which were performed under harmonic vibrations.

This contribution examines two ways of relating vertical accelerations with the creep formula to shed some light to the uncertainty. After introducing the involved methods in Section 2, a case study is presented in Section 3, in which the vertical accelerations obtained through a dynamic train-bridge model are evaluated for vibration-induced creep of a sleeper on this bridge.

2 Methods

2.1 Assessment of vibration-induced creep of ballasted track on vibrating bridge decks

In [10] a framework for assessing vibration induced creep of ballasted track on vibrating bridge decks is proposed. It aims to address the track maintenance requirements which inform the deflection limit Δf_{lim} within a given reference timeframe t_R. Fig. 1 shows the following key steps of the framework:

1. **Limit State Definition**: Establish a limit for lateral deflections, denoted as Δf_{lim}, within a reference timeframe t_R. with an associated number of train passages, N_{pass}.
2. **Track Model Analysis**: Develop a model of the track that includes imperfections. For a given temperature change ΔT, calculate the lateral forces F_L at the sleepers.

3. **Train-Bridge Dynamic Analysis**: Create a dynamic model of the bridge and simulate train passages. For conservative estimates, consider worst-case scenarios.
4. **Postprocessing of accelerations**: Perform postprocessing with peak identification or cycle counting along the track axis or at previously identified critical locations. These algorithms provide pairs of $(\Delta a_C, n_C)$ for counted cycles within predefined acceleration amplitude classes or a sequence of acceleration peaks a_i.
5. **Lateral Displacements for a Single Passage**: At each sleeper location, use the lateral load F_L from the track model and the equivalent postprocessed accelerations, calculate the vibration-induced creep Δf for a single train passage.
6. **Evaluation for Reference Timeframe**: Combine different scenarios and evaluate the condition: $N_{pass} \times \Delta f \leq \Delta f_{lim}$.

In the current contribution the steps 4. and 5. are examined closer and the lateral force F_L will be treated as given, thus sidestepping the need for a lateral track model.

2.2 Vibration-induced creep

Previous experiments [4, 5] have identified the lateral force F_L, the peak amplitudes of vertical acceleration $\hat{a}$ and the number N_{cycl} of acceleration cycles as parameters critical for the vibration induced creep Δf. With these critical parameters, for the vibration-induced creep Δf a formula could be derived for harmonic loading scenarios:

$$\Delta f = \text{sign}\left(\frac{F_L}{F_{L0}}\right) \cdot C_1 \cdot \left|\frac{F_L}{F_{L0}}\right|^{C_2} \cdot \exp\left(C_3 \cdot \frac{\hat{a}}{a_0}\right) \cdot N_{cycl} \qquad (1)$$

The unit-less normalization takes place through $F_{L0} = 1\,\text{kN}$ and $a_0 = 1\,\text{g}$. For a specific laboratory experimental set-up, the values of the constants could be determined as:

$$\begin{aligned} C_1 &= 0.0000009 \\ C_2 &= 3.65 \\ C_3 &= 12.523 \end{aligned} \qquad (2)$$

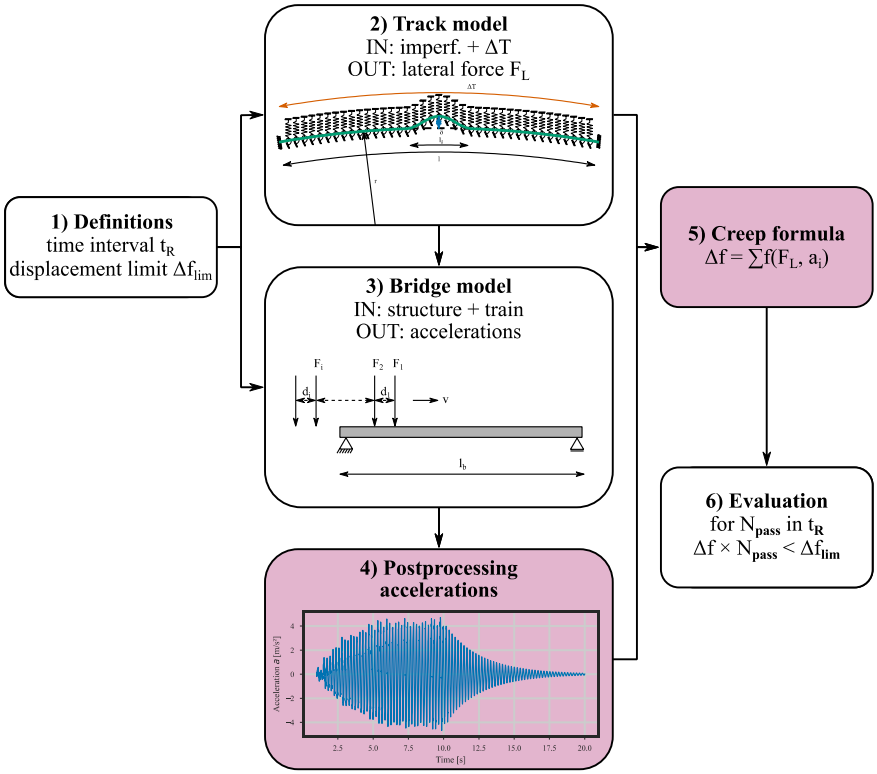

Fig. 1. Flowchart of the method for assessment of vibration-induced lateral creep, taken from [10]. The highlighted parts of the procedure are examined in this contribution.

2.3 Cycle count equivalence

The formula for vibration-induced creep was derived for harmonic vertical accelerations as a function of the lateral force F_L, the peak amplitudes of vertical acceleration $\hat{a}$ and the number N_{cycl}: $\Delta f = f(F_L, \hat{a}, N_{cycl})$. However, the vertical vibrations a bridge deck experiences are not necessarily of harmonic nature. To address non-harmonic vibrations, the creep formula Eq. (1) can be reformulated in two ways:

1. As a summation of single cycles with each an individual peak acceleration amplitude: $\Delta f = \sum_i f(F_L, a_i, 1)$, and
2. as a summation of binned vibration cycles, each with a corresponding acceleration range Δa_C and number n_C of cycles: $\Delta f = \sum_i f(F_L, \Delta a_{C,i}/2, n_{C,i})$.

The acceleration in gravity direction is detrimental to the ballast stability, since this lowers the effective dead weight of the ballast particles which reduces the internal friction between ballast particles and lowers the internal prestress. Therefore,

only the acceleration peaks in downward direction must be considered. Fig. 2 shows illustrations of the equivalence of the three formulations of the vibration-induced creep formula.

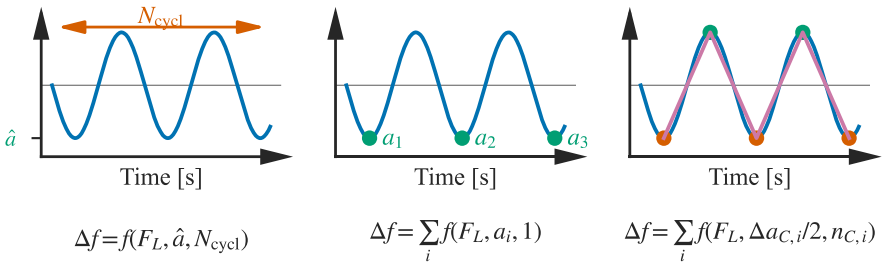

Fig. 2. Equivalence of cycle counting approaches for harmonic excitation. (a) as in the creep formula Eq. 1, (b) as a summation of identified peaks, and (c) as a superposition of counted cycles.

2.4 Peak identification

A peak identification algorithm which identifies the peak downward accelerations between each zero-crossing of the acceleration signal is shown in Table 1. This algorithm assumes that the segment between zero-crossings corresponds to one cycle.

Table 1. Peak identification algorithm.

Algorithm 1: Peak identification	
	Input: acceleration signal $a(t)$ and an optional threshold value T
	Output: identified peaks a_i
1	Find indices of zero crossings, where the signal changes sign.
2	Identify maximum downward acceleration between crossings.
3	Filter identified maxima with a threshold T_P.
4	Output final values of acceleration peaks a_i.

2.5 Rainflow counting

There are numerous cycle counting algorithms that are studied in fatigue analysis. This contribution leverages a three-point rainflow counting method of ASTM E1049-85 [12], which is shown in Table 2.

Table 2. Cycle counting algorithm

Algorithm 2: Cycle counting	
	Input: acceleration signal $a(t)$ and an optional threshold value T
	Output: identified cycle ranges Δa_C and cycle counts n_C
1	Compute first-order differences of the signal.
2	Identify sign changes to identify peaks and valleys as reversal "points"
3	While points has ≥ 3 elements:
4	Let x1, x2, and x3 be the last three points.
5	If X < Y, break.
6	If exactly 3 points, yield half-cycle: (x1, x2), remove first point
7	Else yield full cycle: (x1, x2), remove the (x1, x2, x3), and re-append (x3)
8	Optionally, put the cycles in bins of discrete ranges for Δa
9	Filter identified cycle ranges with the threshold T_C.
10	Output final values of acceleration cycle ranges Δa_C and cycle counts n_C.

3 Case study

This case study compares the two ways of postprocessing acceleration time series and relating the results to the vibration-induced creep formula Eq. (1). First, an acceleration time series is obtained with a dynamic train bridge model (as proposed in Step 3 of the assessment procedure in Section 2.1).

Subsequently the two approaches of postprocessing are carried out (Step 4) and the resulting creep is analyzed (Step 5). For the evaluations of the creep formula, the lateral force F_L is held constant at $F_L = 1.0$ kN, which replaces the lateral track model of Step 2 of the assessment procedure. In the proposed assessment approach, postprocessing acceleration time series and calculating the creep must be carried out for every sleeper location.

For each of the two approaches, the influence of the threshold parameter (T_P.or T_C, respectively) is analyzed. Also, the influence of the optional binning step of the rainflow counting approach is examined.

3.1 Dynamic train-bridge model

A 2D beam-element finite element analysis simulated an ICE4 train traversing an example bridge. The ICE4's dynamic signature peaks at a 9.5m wavelength [13], coinciding with a critical bridge speed of approximately 155 km/h (bridge natural frequency: 4.5 Hz). The train was modeled as moving loads, and time-step integration (0.2 ms, Wilson-theta method) considered the first three bending modes (4.5 Hz, 18.0 Hz, 40.0 Hz). Higher modes were neglected, and the resulting acceleration time series from the node with the highest amplitudes was analyzed. Model parameters are detailed in Table 3; further details in [10].

Table 3. Parameters of the dynamic train-bridge model.

Notation	Parameter	Value
E_b	Elastic modulus	35 GPa
L_s	Bridge span	19.8 m
l_b	Total bridge length	21.0 m
I_b	Second moment of inertia	0.888 m^4
A_b	Area	6.234 m^2
μ	Distributed mass	24.31 t/m
$D_{N,b}$	Nodal spacing	0.6 m
ζ	Modal damping	0.013
v	Train speed	155 km/h
Δt	Time step for integration	0.2 ms

3.2 Peak / Reversals identification

Both algorithms introduced in Section 2 are applied to the acceleration time series of the analysis of the dynamic train-bridge model described in the previous section. Fig. 3 shows the signal and the resulting peaks and reversal points of the algorithms.

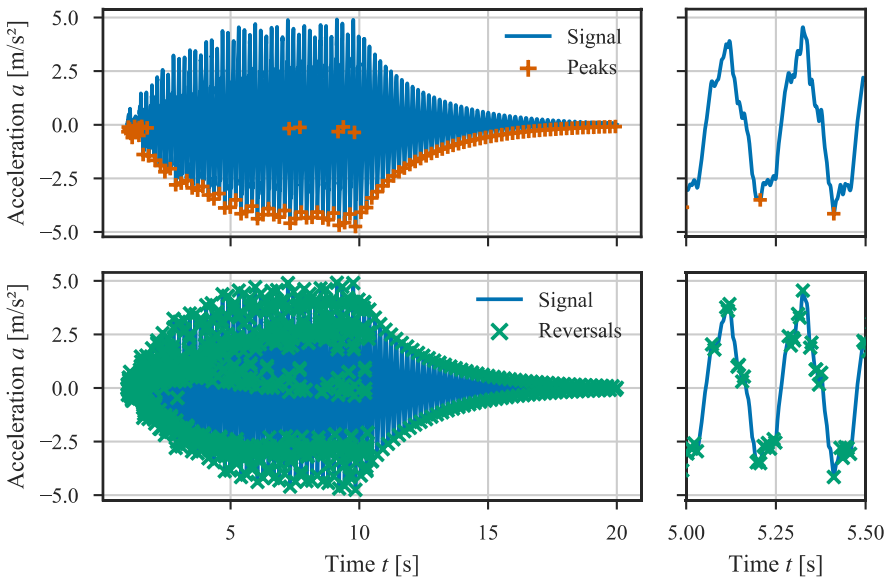

Fig. 3. Acceleration time series of the finite element analysis of the sample bridge, along with identified peaks of Algorithm 1 (top) and reversal points of Algorithm 2 (bottom). Both the complete time span of the simulation (left) and a close up (right) are shown.

3.3 Comparison

Postprocessing a given acceleration time series might yield many small peaks or many cycles with small acceleration ranges, respectively. The number of cycles linearly influences the vibration-induced creep (see Eq. (1), but the acceleration amplitude influences the creep exponentially. To analyze the influence of these two opposing effects, both the results of the postprocessing as well as their effect on the vibration-induced creep are examined.

Fig. 4 (left) compares the histograms of the results of the peak identification (top) and rainflow counting (bottom) algorithms. For the comparison, the peaks a_i have been matched to the half of the scale of the acceleration cycles $\Delta a_{C,i}$, since the peak identification approach operates on peaks a_i, but the cycle count approach divides the accelerations $\Delta a_{C,i}$ by 2 for the application of the creep formula. The rainflow counting yields a very large number of cycles with a small acceleration range.

Fig. 4 (right) compares the vibration-induced creep for different threshold values of T_P.or T_C, below which acceleration peaks or counted cycles are ignored. Increasing the threshold value progressively eliminates the contribution of lower-amplitude acceleration peaks (or cycles) to the calculated creep.

The results for both approaches “Peaks” and “Cycles (unbinned)” differ by 21 % at most. Most of the change in resulting creep happens at acceleration levels $a_i > 3\ \mathrm{m/s^2}$. Additionally, binned cycles with discrete ranges of 1 m/s² (refer to Step 8 of Algorithm 2) is plotted as “Cycles (binned)”. These results differ a lot from the other results, indicating that binning cycles introduces large errors due to rounding to the next discrete acceleration range value.

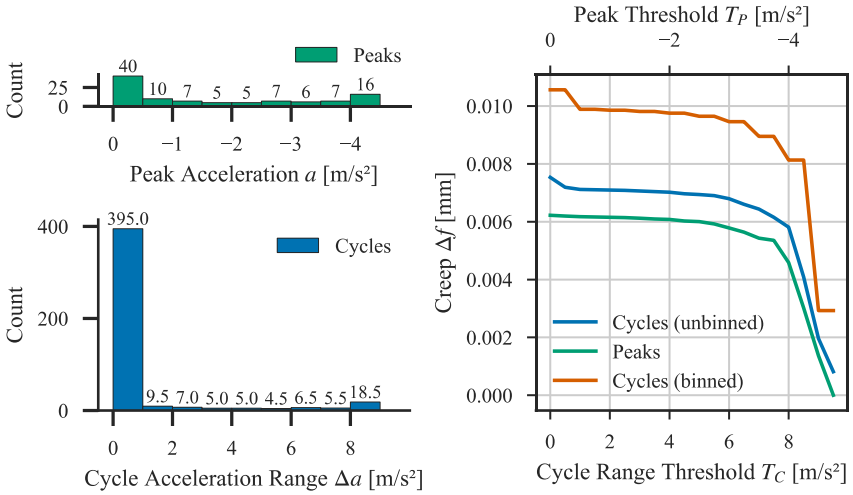

Fig. 4. Histograms of the identified peak accelerations (top left), and cycle counts (bottom left). Accumulated creep over threshold values for both methods (right).

3.4 Creep over train speed

If dynamic analyses are necessitated by the code [3, 13], they usually examine the maximum acceleration over a range of possible train speeds v. Fig. 5 (top) shows such a graph for the bridge and train combination of the case study in steps of 2.5 km/h. Fig. 5 (bottom) shows the vibration induced creep over the train speed. For critical train speeds, creep results vary more than the acceleration amplitudes.

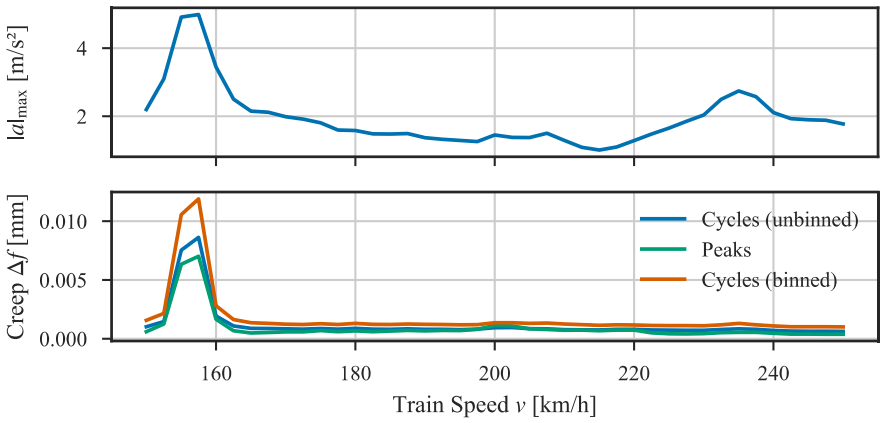

Fig. 5. Maximum acceleration (top) and calculated vibration-induced creep with both methods (bottom) over various train speeds.

4 Discussion

The case study compared different approaches for postprocessing acceleration time series applying the results to the formula for vibration-induced creep.

The examination of different threshold values shows differences in the postprocessing procedures, albeit the most discrepancy occurs between binning and not binning the cycles of the rainflow counting algorithm. Most of the creep is accumulated for peaks $a > 3\ \mathrm{m/s^2}$. or cycles with ranges levels $\Delta a_C > 6\ \mathrm{m/s^2}$.

5 Conclusion

There exist various uncertainties in the proposed assessment framework for vibration-induced creep [10]. The current study was concerned with different postprocessing approaches within this framework. It was shown that the results differ and thus uncertainty persists. Under the boundary conditions of the case study, the unbinned rainflow counting approach yields conservative results.

Future research on this should aim to further quantify the uncertainty and generalize the assessment, utilizing parameter studies [13] or probabilistic analyses [14].

Acknowledgements

The authors would like to acknowledge the financial support of Europe's Rail Joint Undertaking through the project *InBridge4EU — Enhanced Interfaces and train categories for dynamic compatibility assessment of European railway bridges (Grant agreement number 101121765)*.

References

1. Goicolea-Ruigómez J M (2008) Service limit states for railway bridges in new design codes IAPF and Eurocodes. In: *Track-bridge interaction on high-speed railways*. CRC Press pp. 17–28.
2. ERRI Comittee ERRI D214/RP9 Rail bridges for speeds > 200 km/h: Final report., ERRI D214/RP9, (1999).
3. CEN - European Comittee for Standardization *EN 1990:2023-03 Eurocode - Basis of structural and geotechnical design*, EN 1990:2023-03, (2023).
4. Baeßler M, Cuéllar P, Rücker W (2014) The Lateral Stability of Ballasted Tracks on Vibrating Bridge Decks. *International Journal of Railway Technology* 3(2):1–22.
5. Baeßler M (2008) Settlement and stability of ballasted track due to cyclic and dynamic loading (in German). PhD Thesis Technische Universität Berlin, Berlin.
6. Stollwitzer A, Fink J, Malik T (2020) Experimental analysis of damping mechanisms in ballasted track on single-track railway bridges. *Engineering Structures* 220:110982.
7. Heiland T, Hägle M, Triantafyllidis T, Stempniewski L, Stark A (2022) Stiffness contributions of ballast in the context of dynamic analysis of short span railway bridges. *Construction and Building Materials* 360:129536.
8. Chordà-Monsonís J, Romero A, Moliner E, Galvín P, Martínez-Rodrigo M D (2022) Ballast shear effects on the dynamic response of railway bridges. *Engineering Structures* 272:114957.
9. Nakamura T, Momoya Y, Nomura K, Yoshihiko Y (2016) Shaking Table Test Using Full-scale Model for Lateral Resistance Force of Ballasted Tracks During Earthquake. *Procedia Engineering* 143:1100–1107.
10. Baeßler M, Simon P (2025) Ballasted track on vibrating bridge decks: physical mechanisms, empirical findings, and a proposal for assessment. *International Journal of Structural Stability and Dynamics*.
11. Menezes J M (2024) Modelling of the dynamic behaviour of ballast on railway bridges. Master Thesis Universidade do Porto, Porto, Portugal.
12. ASTM International *Standard practices for cycle counting in fatigue analysis*, ASTM E1049-85, (2017).
13. Kohl A, Firus A, Rupp M, Schneider J, Kwapisz M, Vorwagner A, Reiterer M, Vospernig M, Tukhbatullin R, Lombaert G Research Project: Bridge Dynamics; dynamic load model (in German)., Deutsches Zentrum für Schienenverkehrsforschung beim Eisenbahn-Bundesamt, (2024). doi: 10.48755/DZSF.240009.01.
14. Ferreira G, Montenegro P, Andersson A, Henriques A A, Karoumi R, Calçada R (2024) Critical analysis of the current Eurocode deck acceleration limit for evaluating running safety in ballastless railway bridges. *Engineering Structures* 312:118127.